

Production of $f_2(1270)$ meson in pp collisions at the LHC via gluon-gluon fusion in the k_t -factorization approach

Piotr Lebiedowicz^{1,*} and Antoni Szczurek^{b1,‡}

¹*Institute of Nuclear Physics Polish Academy of Sciences,
Radzikowskiego 152, PL-31342 Kraków, Poland*

Abstract

We calculate inclusive cross section for $f_2(1270)$ tensor meson production via color singlet gluon-gluon fusion in the k_t -factorization approach with unintegrated gluon distribution functions (UGDFs). The process may be potentially interesting in the context of searches for saturation effects. The energy-momentum tensor, equivalent to helicity-2 coupling, and helicity-0 coupling are used for the $g^*g^* \rightarrow f_2(1270)$ vertex. Two somewhat different parametrizations of helicity-2 and helicity-0 tensorial structure from the literature are used in our calculations. Some parameters are extracted from $\gamma\gamma \rightarrow f_2(1270) \rightarrow \pi\pi$ reactions. Different modern UGDFs from the literature are used. The results strongly depend on the parametrization of the $g^*g^* \rightarrow f_2(1270)$ form factor. Our results for transverse momentum distributions of f_2 are compared to preliminary ALICE data. We can obtain agreement with the data only at larger $f_2(1270)$ transverse momenta only for some parametrizations of the $g^*g^* \rightarrow f_2(1270)$ form factor. No obvious sign of the onset of saturation is possible. At low transverse momenta one needs to include also the $\pi\pi$ final-state rescattering. The agreement with the ALICE data can be obtained by adjusting probability of formation and survival of $f_2(1270)$ in a harsh quark-gluon and multipion environment. The pomeron-pomeron fusion mechanism is discussed in addition and results are quantified.

arXiv:2007.12485v2 [hep-ph] 6 Aug 2020

^b Also at *College of Natural Sciences, Institute of Physics, University of Rzeszów, Pigońia 1, PL-35310 Rzeszów, Poland.*

* Piotr.Lebiedowicz@ifj.edu.pl

‡ Antoni.Szczurek@ifj.edu.pl

I. INTRODUCTION

The mechanism of $f_2(1270)$ meson production in proton-proton collisions at high energies was not carefully studied so far. In the PYTHIA event generator $f_2(1270)$ is not produced in a primary fragmentation process but occurs only in decays, e.g. $J/\psi \rightarrow f_2(1270)\omega$, $D_s^\pm \rightarrow f_2(1270)\pi^\pm$, $B^\pm \rightarrow \tau^\pm\nu_\tau/\bar{\nu}_\tau f_2(1270)$. The corresponding branching fractions are rather small so one cannot expect large contributions. On the other hand it is rather difficult to observe $f_2(1270)$ experimentally. The dominant, and relatively easy, decay channel is $f_2(1270) \rightarrow \pi^+\pi^-$. Then the signal is on a huge non-reduceable $\pi^+\pi^-$ background. So far only STAR [1] and ALICE [2] undertook experimental efforts. Some time ago [3] it was suggested that the gluon-gluon fusion could be the dominant production mechanism. Certainly this interesting working hypothesis requires further elaboration and experimental confirmation.

In the present paper we follow the idea from [3] and try to shed new light on the situation. We will apply the k_t -factorization approach successfully used for χ_c quarkonium production [4, 5], for $\eta_c(1S, 2S)$ production [6, 7], and recently for $f_0(980)$ production [8] in proton-proton collisions. In this study, we focus on the production of $f_2(1270)$ meson in pp collisions. Recently the production of f_2 was also studied in $\gamma p \rightarrow f_2 p$ reaction [9]. The $g^*g^* \rightarrow f_2(1270)$ vertex is not known a priori. We will try to verify the hypothesis of the dominance of the helicity-2 component, the coupling of spin-2 meson to the energy-momentum tensor [3], by comparing our results to the preliminary ALICE data [2]. We shall use modern unintegrated gluon distributions from the literature.

The tensor-meson dominance for energy-momentum tensor (see e.g. [3]) is a possibility used already in $\gamma\gamma \rightarrow f_2(1270)$ subprocess [10] for two on-shell photons. In [11] two tensor structures corresponding to $\Gamma^{(0)}$ helicity-0 and $\Gamma^{(2)}$ helicity-2 couplings were found and their strength was determined from the comparison to the Belle data for the $\gamma\gamma \rightarrow \pi\pi$ reactions. The data with the on-shell photons require dominance of helicity-2 coupling over helicity-0 coupling; see Refs. [12–14]. The $\gamma^*\gamma \rightarrow f_2(1270)$ coupling was discussed in [15–18]. The f_2 meson transition form factors were discussed e.g. in [19, 20] in the quark model and in the asymptotic regime of one large virtuality, respectively. The differential cross section for the process $\gamma^*\gamma \rightarrow \pi^0\pi^0$ in e^+e^- scattering up to $Q^2 = 30 \text{ GeV}^2$ was studied by the Belle Collaboration [21]. The transition form factor of the $f_0(980)$ meson and helicity-0, -1, and -2 transition form factors of the $f_2(1270)$ meson were extracted there. We will also use tensorial structures for the $\gamma^*\gamma^* \rightarrow f_2(1270)$ vertex from [22] (see also Ref. [23]). Recently, some numerical results for the helicity amplitudes of $\gamma^*\gamma^* \rightarrow \pi\pi$ that, include $f_2(1270)$, depending of the photon virtualities, were presented in [24, 25].

II. SOME DETAILS OF THE MODEL CALCULATIONS

A. $\gamma^*\gamma^* \rightarrow f_2(1270)$ vertex

1. Ewerz-Maniatis-Nachtmann vertex (EMN)

In [11] the $f_2\gamma\gamma$ vertex for ‘on-shell’ f_2 meson and real photons was considered; see Eq. (3.39) of [11] and the discussion in Sec. 5.3 therein. In this approach the photon-

photon- f_2 vertices come from Lagrangian formulation for both on-shell photons and fulfil gauge invariance. The same model is used then off-mass shell for virtual photons.

Here we are interested in $\gamma^*(Q_1^2)\gamma^*(Q_2^2) \rightarrow f_2(1270)$ process, thus to describe the dependence on photon virtualities we should introduce the vertex form factors $F^{(0)}(Q_1^2, Q_2^2)$ and $F^{(2)}(Q_1^2, Q_2^2)$ for the helicity-0 coupling and the helicity-2 coupling, respectively.

Then the $\gamma^*\gamma^* \rightarrow f_2(1270)$ vertex, including the form factors $F^{(\Lambda)}(Q_1^2, Q_2^2)$, can be parametrized as

$$\begin{aligned} \Gamma_{\mu\nu\kappa\lambda}^{(f_2\gamma\gamma)}(q_1, q_2) &= 2a_{f_2\gamma\gamma} \Gamma_{\mu\nu\kappa\lambda}^{(0)}(q_1, q_2) F^{(0)}(Q_1^2, Q_2^2) \\ &\quad - b_{f_2\gamma\gamma} \Gamma_{\mu\nu\kappa\lambda}^{(2)}(q_1, q_2) F^{(2)}(Q_1^2, Q_2^2), \end{aligned} \quad (2.1)$$

with two rank-four tensor functions,

$$\Gamma_{\mu\nu\kappa\lambda}^{(0)}(q_1, q_2) = \left[(q_1 \cdot q_2) g_{\mu\nu} - q_{2\mu} q_{1\nu} \right] \left[q_{1\kappa} q_{2\lambda} + q_{2\kappa} q_{1\lambda} - \frac{1}{2} (q_1 \cdot q_2) g_{\kappa\lambda} \right], \quad (2.2)$$

$$\begin{aligned} \Gamma_{\mu\nu\kappa\lambda}^{(2)}(q_1, q_2) &= (q_1 \cdot q_2) (g_{\mu\kappa} g_{\nu\lambda} + g_{\mu\lambda} g_{\nu\kappa}) + g_{\mu\nu} (q_{1\kappa} q_{2\lambda} + q_{2\kappa} q_{1\lambda}) \\ &\quad - q_{1\nu} q_{2\lambda} g_{\mu\kappa} - q_{1\nu} q_{2\kappa} g_{\mu\lambda} - q_{2\mu} q_{1\lambda} g_{\nu\kappa} - q_{2\mu} q_{1\kappa} g_{\nu\lambda} \\ &\quad - [(q_1 \cdot q_2) g_{\mu\nu} - q_{2\mu} q_{1\nu}] g_{\kappa\lambda}; \end{aligned} \quad (2.3)$$

see Eqs. (3.18)–(3.22) of [11].

To obtain $a_{f_2\gamma\gamma}$ and $b_{f_2\gamma\gamma}$ in (2.1) we use the experimental value of the radiative decay width

$$\begin{aligned} \Gamma(f_2 \rightarrow \gamma\gamma) &= (2.93 \pm 0.40) \text{ keV}, \\ \text{helicity zero contribution} &\approx 9\% \text{ of } \Gamma(f_2 \rightarrow \gamma\gamma), \end{aligned} \quad (2.4)$$

as quoted for the preferred solution III in Table 3 of [14]. Using the decay rate from (5.28) of [11]

$$\Gamma(f_2 \rightarrow \gamma\gamma) = \frac{m_{f_2}}{80\pi} \left(\frac{1}{6} m_{f_2}^6 |a_{f_2\gamma\gamma}|^2 + m_{f_2}^2 |b_{f_2\gamma\gamma}|^2 \right), \quad (2.5)$$

and assuming $a_{f_2\gamma\gamma} > 0$ and $b_{f_2\gamma\gamma} > 0$, we find

$$a_{f_2\gamma\gamma} = \alpha_{\text{em}} \times 1.17 \text{ GeV}^{-3}, \quad (2.6)$$

$$b_{f_2\gamma\gamma} = \alpha_{\text{em}} \times 2.46 \text{ GeV}^{-1}, \quad (2.7)$$

where $\alpha_{\text{em}} = e^2/(4\pi) \simeq 1/137$ is the electromagnetic coupling constant.

2. Pascalutsa-Pauk-Vanderhaeghen vertex (PPV)

In Refs. [19, 22, 23] it was shown that the most general amplitude for the process $\gamma^*(q_1, \lambda_1) + \gamma^*(q_2, \lambda_2) \rightarrow f_2(\Lambda)$, describing the transition from an initial state of two virtual photons to a tensor meson f_2 ($J^{PC} = 2^{++}$) with the mass m_{f_2} and helicity $\Lambda = \pm 2, \pm 1, 0$, involves five independent structures (invariant amplitudes).

In the formalism presented in [22] the $\gamma^* \gamma^* \rightarrow f_2(1270)$ vertex was parametrized as

$$\begin{aligned} \Gamma_{\mu\nu\kappa\lambda}^{(f_2\gamma\gamma)}(q_1, q_2) = & 4\pi\alpha_{\text{em}} \left\{ \left[R_{\mu\kappa}(q_1, q_2)R_{\nu\lambda}(q_1, q_2) + \frac{s}{8X} R_{\mu\nu}(q_1, q_2)(q_1 - q_2)_\kappa (q_1 - q_2)_\lambda \right] \right. \\ & \times \frac{\nu}{m_{f_2}} T^{(2)}(Q_1^2, Q_2^2) \\ & + R_{\nu\kappa}(q_1, q_2)(q_1 - q_2)_\lambda \left(q_{1\mu} + \frac{Q_1^2}{\nu} q_{2\mu} \right) \frac{1}{m_{f_2}} T^{(1)}(Q_1^2, Q_2^2) \\ & + R_{\mu\kappa}(q_1, q_2)(q_2 - q_1)_\lambda \left(q_{2\nu} + \frac{Q_2^2}{\nu} q_{1\nu} \right) \frac{1}{m_{f_2}} T^{(1)}(Q_2^2, Q_1^2) \\ & + R_{\mu\nu}(q_1, q_2)(q_1 - q_2)_\kappa (q_1 - q_2)_\lambda \frac{1}{m_{f_2}} T^{(0,T)}(Q_1^2, Q_2^2) \\ & \left. + \left(q_{1\mu} + \frac{Q_1^2}{\nu} q_{2\mu} \right) \left(q_{2\nu} + \frac{Q_2^2}{\nu} q_{1\nu} \right) (q_1 - q_2)_\kappa (q_1 - q_2)_\lambda \frac{1}{m_{f_2}^3} T^{(0,L)}(Q_1^2, Q_2^2) \right\}, \quad (2.8) \end{aligned}$$

where photons with four-momenta q_1 and q_2 have virtualities, $Q_1^2 = -q_1^2$ and $Q_2^2 = -q_2^2$, $s = (q_1 + q_2)^2 = 2\nu - Q_1^2 - Q_2^2$, $X = \nu^2 - q_1^2 q_2^2$, $\nu = (q_1 \cdot q_2)$, and

$$R_{\mu\nu}(q_1, q_2) = -g_{\mu\nu} + \frac{1}{X} \left[\nu (q_{1\mu} q_{2\nu} + q_{2\mu} q_{1\nu}) - q_1^2 q_{2\mu} q_{2\nu} - q_2^2 q_{1\mu} q_{1\nu} \right]. \quad (2.9)$$

In Eq. (2.8) $T^{(\Lambda)}(Q_1^2, Q_2^2)$ are the $\gamma^* \gamma^* \rightarrow f_2(1270)$ transition form factors for $f_2(1270)$ helicity Λ . For the case of helicity zero, there are two form factors depending on whether both photons are transverse (superscript T) or longitudinal (superscript L).

We can express the transition form factors as

$$T^{(\Lambda)}(Q_1^2, Q_2^2) = F^{(\Lambda)}(Q_1^2, Q_2^2) T^{(\Lambda)}(0, 0). \quad (2.10)$$

In the limit $Q_{1,2}^2 \rightarrow 0$ only $T^{(0,T)}$ and $T^{(2)}$ contribute and their values at $Q_{1,2}^2 \rightarrow 0$ determine the two-photon decay width of $f_2(1270)$ meson.

Comparing the two approaches given by (2.1) and (2.8)–(2.10) for both real photons ($Q_1^2 = Q_2^2 = 0$) and at $\sqrt{s} = m_{f_2}$ we found the correspondence

$$4\pi\alpha_{\text{em}} T^{(0,T)}(0, 0) = -a_{f_2\gamma\gamma} \frac{m_{f_2}^3}{2}, \quad (2.11)$$

$$4\pi\alpha_{\text{em}} T^{(2)}(0, 0) = -b_{f_2\gamma\gamma} 2m_{f_2}. \quad (2.12)$$

B. $g^* g^* \rightarrow f_2(1270)$ vertex

We will apply the formalism for the $\gamma^* \gamma^* \rightarrow f_2$ vertices discussed in Sec. II A. This means that the $g^* g^* \rightarrow f_2(1270)$ vertex has the same form as that for the $\gamma^* \gamma^* \rightarrow f_2(1270)$ vertex, but with the replacement (2.21).

Because $f_2(1270)$ is extended, finite size object one can expect in addition a form factor(s) $F(Q_1^2, Q_2^2)$ associated with the gluon virtualities for the $g^* g^* \rightarrow f_2$ vertex¹. In the

¹ In general the form factors for different tensorial structures can be different.

present letter the form factor, identical for $\Lambda = 0$ and $\Lambda = 2$, is parametrized in different ways as:

$$F(Q_1^2, Q_2^2) = \frac{\Lambda_M^2}{Q_1^2 + Q_2^2 + \Lambda_M^2}, \quad (2.13)$$

$$F(Q_1^2, Q_2^2) = \left(\frac{\Lambda_D^2}{Q_1^2 + Q_2^2 + \Lambda_D^2} \right)^2, \quad (2.14)$$

$$F(Q_1^2, Q_2^2) = \frac{\Lambda_1^2}{Q_1^2 + \Lambda_1^2} \frac{\Lambda_1^2}{Q_2^2 + \Lambda_1^2}, \quad (2.15)$$

$$F(Q_1^2, Q_2^2) = \frac{\Lambda_1^4}{(Q_1^2 + \Lambda_1^2)^2} \frac{\Lambda_2^4}{(Q_2^2 + \Lambda_2^2)^2}, \quad (2.16)$$

where Λ 's above are parameters whose value is expected to be close to the resonance mass [19]. In the case of non-factorized form factors, monopole (2.13) and dipole (2.14), we use $\Lambda_M = \Lambda_D = m_{f_2}$. The values of Λ_1 in (2.15) and Λ_2 in (2.16) are expected to be of order of 1 GeV. The results for different forms of the form factors (2.13)–(2.16) are presented in Fig. 3. The results strongly depend on the parametrization chosen and the value of the corresponding parameter.

C. k_t -factorization approach

In Fig. 1 we show a generic Feynman diagram for $f_2(1270)$ meson production in proton-proton collision via gluon-gluon fusion. This diagram illustrates the situation adequate for the k_t -factorization calculations used in the present paper.

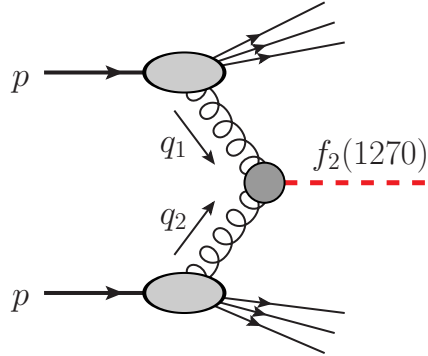


FIG. 1. General diagram for inclusive $f_2(1270)$ production via gluon-gluon fusion in proton-proton collisions.

The differential cross section for inclusive $f_2(1270)$ meson production via the $g^*g^* \rightarrow f_2(1270)$ fusion in the k_t -factorization approach can be written as:

$$\frac{d\sigma}{dyd^2\mathbf{p}} = \int \frac{d^2\mathbf{q}_1}{\pi q_1^2} \mathcal{F}_g(x_1, \mathbf{q}_1^2) \int \frac{d^2\mathbf{q}_2}{\pi q_2^2} \mathcal{F}_g(x_2, \mathbf{q}_2^2) \delta^{(2)}(\mathbf{q}_1 + \mathbf{q}_2 - \mathbf{p}) \frac{\pi}{(x_1 x_2 s)^2} \overline{|\mathcal{M}_{g^*g^* \rightarrow f_2}|^2}. \quad (2.17)$$

Here \mathbf{q}_1 , \mathbf{q}_2 and \mathbf{p} denote the transverse momenta of the gluons and the $f_2(1270)$ meson, respectively. The f_2 meson is on-shell and its momentum satisfies $p^2 = m_{f_2}^2$. $\mathcal{M}_{g^*g^* \rightarrow f_2}$ is the matrix element for off-shell gluons for the hard subprocess and \mathcal{F}_g are the gluon unintegrated distribution functions (UGDFs) for colliding protons. The UGDFs depend on gluon longitudinal momentum fractions $x_{1,2} = m_T \exp(\pm y) / \sqrt{s}$ and $\mathbf{q}_1^2, \mathbf{q}_2^2$ entering the hard process. In principle, they can depend also on factorization scales $\mu_{F,i}^2, i = 1, 2$. It is reasonable to assume $\mu_{F,1}^2 = \mu_{F,2}^2 = m_T^2$. Here m_T is transverse mass of the produced $f_2(1270)$ meson; $m_T = \sqrt{\mathbf{p}^2 + m_{f_2}^2}$. The $\delta^{(2)}$ function in Eq. (2.17) can be easily eliminated by introducing $\mathbf{q}_1 + \mathbf{q}_2$ and $\mathbf{q}_1 - \mathbf{q}_2$ transverse momenta [4].

The off-shell matrix element can be written as (we restore the color-indices a and b)

$$\mathcal{M}^{ab} = \frac{q_{1t}^\mu q_{2t}^\nu}{|\mathbf{q}_1||\mathbf{q}_2|} \mathcal{M}_{\mu\nu}^{ab} = \frac{q_{1+} q_{2-}}{|\mathbf{q}_1||\mathbf{q}_2|} n^{+\mu} n^{-\nu} \mathcal{M}_{\mu\nu}^{ab} = \frac{x_1 x_2 s}{2|\mathbf{q}_1||\mathbf{q}_2|} n^{+\mu} n^{-\nu} \mathcal{M}_{\mu\nu}^{ab} \quad (2.18)$$

with the lightcone components of gluon momenta $q_{1+} = x_1 \sqrt{s/2}$, $q_{2-} = x_2 \sqrt{s/2}$. Here the matrix-element reads

$$\mathcal{M}_{\mu\nu} = \Gamma_{\mu\nu\kappa\lambda}^{(f_2 gg)}(q_{1t}, q_{2t}) (\epsilon^{(f_2)\kappa\lambda}(p))^*, \quad (2.19)$$

where $\epsilon^{(f_2)}$ is the polarization tensor for the $f_2(1270)$ meson.

In the k_t -factorization approach in [3] the matrix element squared (for energy-momentum tensor coupling) was written as:

$$\begin{aligned} & \overline{|\mathcal{M}_{g^*g^* \rightarrow f_2}|^2} \\ &= \frac{1}{(N_c^2 - 1)^2} \sum_{a,b} \frac{q_{1t} \mu_1}{q_{1t}} \frac{q_{2t} \nu_1}{q_{2t}} V_{ab}^{\alpha_1 \beta_1 \mu_1 \nu_1}(q_1, q_2) P_{\alpha_1 \beta_1, \alpha_2 \beta_2}^{(2)}(p) \frac{q_{1t} \mu_2}{q_{1t}} \frac{q_{2t} \nu_2}{q_{2t}} \left(V_{ab}^{\alpha_2 \beta_2 \mu_2 \nu_2}(q_1, q_2) \right)^* \\ &= \frac{1}{(N_c^2 - 1) \kappa^2} P_{\alpha_1 \beta_1, \alpha_2 \beta_2}^{(2)}(p) H_{\perp}^{\alpha_1 \beta_1}(q_{1t}, q_{2t}) H_{\perp}^{\alpha_2 \beta_2}(q_{1t}, q_{2t}) \left(\frac{x_1 x_2 s}{2q_{1t} q_{2t}} \right)^2, \end{aligned} \quad (2.20)$$

where N_c is the number of colors, $V_{ab}^{\alpha\beta\mu\nu}$ is the $gg \rightarrow f_2$ vertex² (see Eq. (A1) of [3]), and $\kappa \approx \mathcal{O}(0.1 \text{ GeV})$ is to be fixed by experiment. The explicit forms for the spin-2 projector $P^{(2)}$ and $H_{\perp}^{\alpha\beta}$ functions (with transverse components) are given in [3]. In the above formula (2.20) α_s is not explicit but is hidden in the normalization constant. In our calculation we will make α_s explicit, i.e. include its running with relevant scales. We have checked that the approach in [3] is equivalent to the approach with the helicity-2 EMN vertex function (2.3) when ignoring running of α_s and vertex form factor $F(Q_1^2, Q_2^2)$. Having $F(Q_1^2, Q_2^2)$ is crucial for description of transverse momentum distribution of $f_2(1270)$ as will be discussed in the result section.

The $g^*g^* \rightarrow f_2(1270)$ coupling entering in the matrix element squared can be obtained from that for the $\gamma^*\gamma^* \rightarrow f_2(1270)$ coupling by the following replacement:

$$\alpha_{\text{em}}^2 \rightarrow \alpha_s^2 \frac{1}{4N_c(N_c^2 - 1)} \frac{1}{(\langle e_q^2 \rangle)^2}. \quad (2.21)$$

² Please note that the order of Lorentz indices here (and in Ref. [3]) is different than in Eq. (2.3).

Here $(\langle e_q^2 \rangle)^2 = 25/162$ for the $\frac{1}{\sqrt{2}}(u\bar{u} + d\bar{d})$ flavor structure assumed for $f_2(1270)$.

In realistic calculations the running of strong coupling constants must be included. In our numerical calculations presented below the renormalization scale is taken in the form:

$$\alpha_s^2 \rightarrow \alpha_s(\max\{m_T^2, q_1^2\}) \alpha_s(\max\{m_T^2, q_2^2\}). \quad (2.22)$$

The Shirkov-Solovtsov prescription [26] is used to extrapolate down to small renormalization scales relevant for the $f_2(1270)$ production for the ALICE kinematics.

D. A simple $\pi\pi$ final-state rescattering model

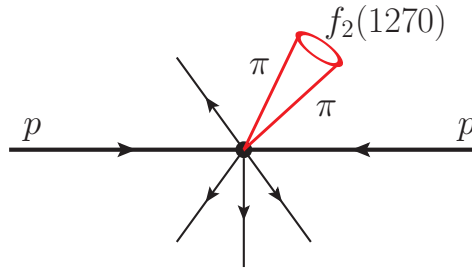


FIG. 2. General diagram for the $\pi\pi$ final-state rescattering leading to $f_2(1270)$ production in proton-proton collisions.

As will be shown in the present paper the $g^*g^* \rightarrow f_2(1270)$ mechanism is insufficient at low $f_2(1270)$ transverse momenta therefore we consider also a final-state rescattering of produced pions. The general diagram representing the $\pi\pi$ rescattering is shown in Fig. 2. Both $\pi^+\pi^-$ and $\pi^0\pi^0$ rescatterings may lead to the production of the $f_2(1270)$ meson as an effect of final state resonance interactions.

The distribution of pions will be not calculated here but instead we will use a Lévy parametrization of the inclusive π^0 cross section proposed in [27] for $\sqrt{s} = 7$ TeV. At the ALICE energies and midrapidities we assume the following relation:

$$\frac{d\sigma^{\pi^+}}{dydp_t}(y, p_t) = \frac{d\sigma^{\pi^-}}{dydp_t}(y, p_t) = \frac{d\sigma^{\pi^0}}{dydp_t}(y, p_t) \quad (2.23)$$

to be valid.

Our approach here is similar in spirit to color evaporation approach considered, e.g., in [8, 28]. In our approach here we do not include possible $\pi\pi$ correlation functions. They are discussed usually at very small relative momentum. For identical particles ($\pi^0\pi^0$ in our case) this is discussed usually in the context of Bose-Einstein correlations. The non-identical particle correlations ($\pi^+\pi^-$ in our case) is less popular but also very interesting [29, 30]. To form the resonance the two pions must be produced in the $\pi\pi$ invariant mass window corresponding to the $f_2(1270)$ meson and close in space one to each other. Including explicitly the second condition would require knowledge of the space-time development of the hadronization process and goes far beyond the present study devoted

to the $g^*g^* \rightarrow f_2(1270)$ mechanism. Instead we write the number of produced $f_2(1270)$ per event as

$$N^{f_2} = \int dy_1 dp_{1t} \int dy_2 dp_{2t} \int \frac{d\phi_1}{2\pi} \frac{d\phi_2}{2\pi} \frac{dN^\pi}{dy_1 dp_{1t}} \frac{dN^\pi}{dy_2 dp_{2t}} P_{\pi\pi \rightarrow f_2}, \quad (2.24)$$

where $dN^\pi/(dydp_t)$ is number of pions per interval of rapidity and transverse momentum. Here for $\frac{dN^\pi}{dy_1 dp_{1t}}$ and $\frac{dN^\pi}{dy_2 dp_{2t}}$ we use the Tsallis parametrization of π^0 at $\sqrt{s} = 7$ TeV from [27]; see Eq. (2) of [27] and fit parameters in Table 3 therein. In Eq. (2.24) $P_{\pi\pi \rightarrow f_2}$ parametrizes probability of the $\pi^+\pi^-$ and $\pi^0\pi^0$ formation of $f_2(1270)$ as well as probability of its survival in a dense hadronic system. It will be treated here as a free parameter adjusted to the $f_2(1270)$ data from [2]. The distribution $dN^{f_2}/(dydp_t)$ is obtained then by calculating y and p_t of the $f_2(1270)$ meson and binning in these variables.

The effect of hadronic rescattering in high-energy pp collisions was discussed very recently in [31] and the application is being developed and will be implemented to PYTHIA event generator.

III. NUMERICAL RESULTS

To convert to the number of $f_2(1270)$ mesons per event, as was presented in Ref. [2], we use the following relation:

$$\frac{dN}{dp_t} = \frac{1}{\sigma_{\text{inel}}} \frac{d\sigma}{dp_t}. \quad (3.1)$$

The inelastic cross section for $\sqrt{s} = 7$ TeV was measured at the LHC and is:

$$\sigma_{\text{inel}} = 73.15 \pm 1.26 \text{ (syst.) mb}, \quad (3.2)$$

$$\sigma_{\text{inel}} = 71.34 \pm 0.36 \text{ (stat.)} \pm 0.83 \text{ (syst.) mb}, \quad (3.3)$$

as obtained by the TOTEM [32] and ATLAS [33] collaborations, respectively. In our calculations we take $\sigma_{\text{inel}} = 72.5$ mb.

In Fig. 3 we present the $f_2(1270)$ meson transverse momentum distributions at $\sqrt{s} = 7$ TeV and $|y| < 0.5$ together with the preliminary ALICE data from [2]. Here, for the color-singlet gluon-gluon fusion mechanism, we used the JH UGDF from [34].³ We show results for two different $g^*g^* \rightarrow f_2$ vertices discussed in Sec. II A, EMN (left panel) and PPV (right panel), and for different forms of parametrization form factor $F(Q_1^2, Q_2^2)$ given by Eqs. (2.13)–(2.16) and (2.10). The results strongly depend on the parametrization of the form factor. Assuming the cut-off parameter to be close to the $f_2(1270)$ mass the forms (2.13) and (2.15) can be excluded as they overestimates the ALICE data at larger p_t .

Fig. 4 shows that there is some difference in the role of $\Lambda = 0, 2$ contributions for the EMN and PPV vertices. In the formalism of [22] [see the PPV vertex (2.8)] there is no interference between so-called $\Lambda = 0, T$ and $\Lambda = 2$ terms while the naive use of the formalism from [11] [see the EMN vertex (2.1)] generates some interference effects.

³ This type of UGD has been obtained by Hautmann and Jung [34] from a description of precise HERA data on deep inelastic structure function by a solution of the CCFM evolution equation [35–37]. This UGDF is available from the CASCADE Monte Carlo code [38]. We use “JH-2013-set2” of Ref. [34], which we label as “JH UGDF”.

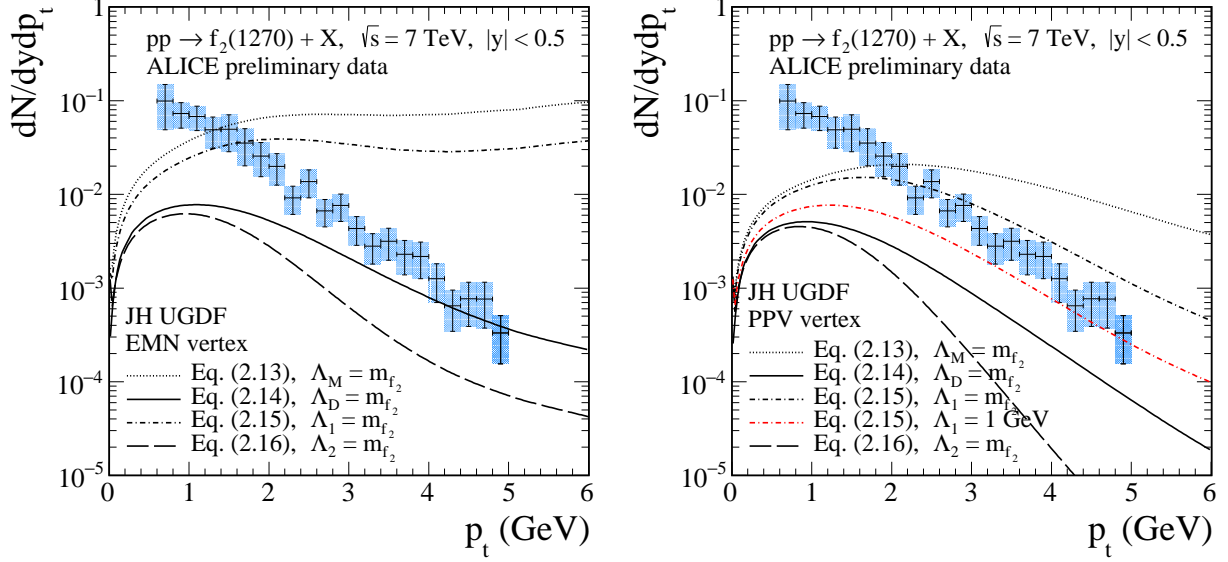


FIG. 3. The $f_2(1270)$ meson transverse momentum distributions at $\sqrt{s} = 7$ TeV and $|y| < 0.5$. The preliminary ALICE data from [2] are shown for comparison. The results for the EMN (left panel) and PPV (right panel) $g^*g^* \rightarrow f_2(1270)$ vertex for different parametrizations of $F(Q_1^2, Q_2^2)$ form factor (2.13)–(2.16) are shown. In this calculation the JH UGDF was used.

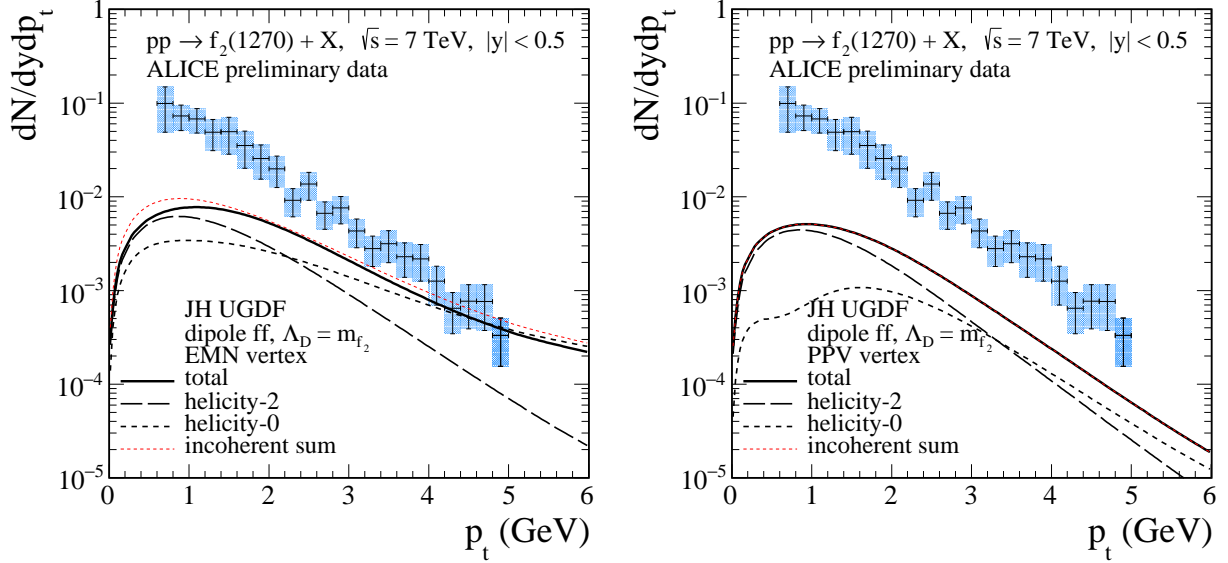


FIG. 4. The $f_2(1270)$ meson transverse momentum distributions at $\sqrt{s} = 7$ TeV and $|y| < 0.5$ together with the preliminary ALICE data from [2]. Shown are the results calculated in the two approaches, EMN (left panel) and PPV (right panel), for the helicity-0 and helicity-2 components separately and their coherent sum (total). The dotted line corresponds to incoherent sum of the two helicity components. In this calculation we used dipole form factor parametrization (2.14) with $\Lambda_D = m_{f_2}$.

Different couplings (independent invariant amplitudes) lead to different shapes of the

transverse momentum distributions. The shape could be verified by experimental data.

In the left panel of Fig 5 we show results for the KMR UGDF.⁴ The KMR UGDF (dashed lines) gives smaller cross section than the JH UGDF (solid lines). The results for both UGDFs coincide for large p_t . The larger the $f_2(1270)$ transverse momentum the larger the range of gluon transverse momenta q_{1t} and/or q_{2t} are probed. This means that at larger f_2 transverse momenta one enters a more perturbative region.

In the right panel of Fig 5 we show the results with the Gaussian smearing of collinear GDF, often used in the context of TMDs, for different smearing parameter $\sigma_0 = 0.25, 0.5, 1.0$ GeV. The GJR08VFNS(LO) collinear GDF [42] was used for this purpose. As expected the shape of $d\sigma/dp_t$ strongly depends on the value of the smearing parameter σ_0 used in the calculation. The speed of $d\sigma/dp_t$ approaching to zero for $p_t \rightarrow 0$ strongly depends on the value of σ_0 . It is impossible to describe simultaneously $p_t < 1$ GeV and $p_t > 1$ GeV regions with the same value of σ_0 . This illustrates the generic situation with all UGDFs.

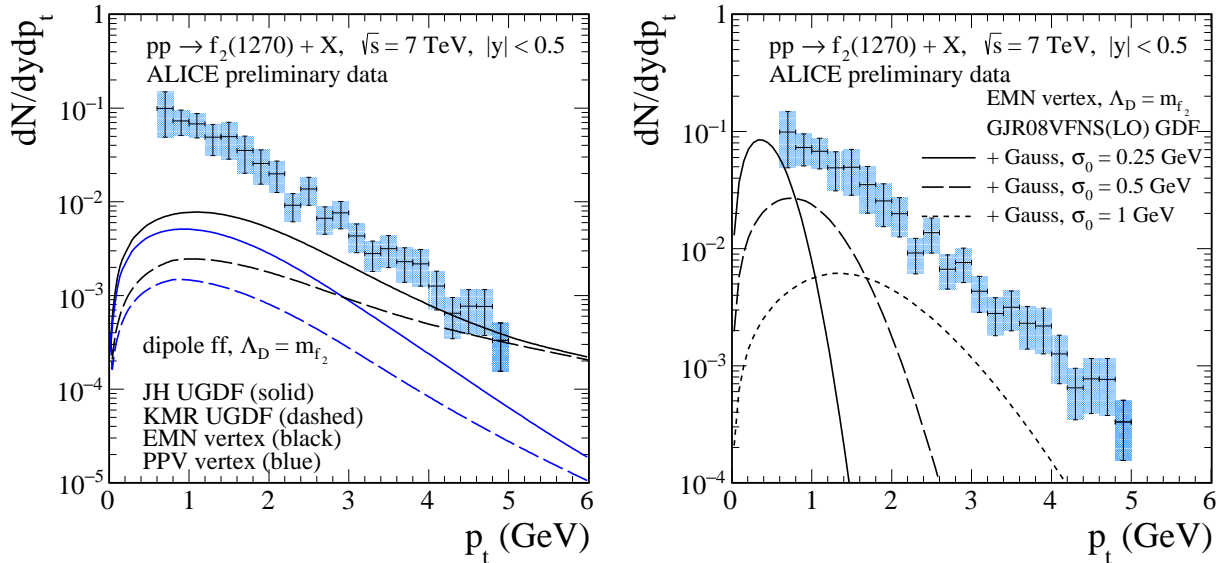


FIG. 5. The $f_2(1270)$ meson transverse momentum distributions at $\sqrt{s} = 7$ TeV and $|y| < 0.5$ together with the preliminary ALICE data from [2]. In the left panel results for two different UGDFs, JH (solid lines) and KMR (dashed lines), are shown. In the right panels we show the dependence on the Gaussian smearing parameter σ_0 for the GJR08VFNS(LO) GDF [42]. Here the EMN vertex discussed in Sec. II A 1 and the dipole form factor (2.14) with $\Lambda_D = m_{f_2}$ were used.

In Fig. 6 we present $d^2\sigma/dq_{1t}dq_{2t}$ for the EMN (left panel) and PPV (right panel) $g^*g^* \rightarrow f_2(1270)$ vertices. Here the JH UGDF was used. The maximal contributions come from the region of rather small gluon transverse momenta $q_{1t}, q_{2t} \lesssim 1$ GeV. It is easy to check (numerically) that the larger- p_t region ($p_t > 2$ GeV) is sensitive to $q_{1t}, q_{2t} > 1$ GeV where perturbative methods apply. At low p_t there is a nonnegligible contribution from the nonperturbative region of UGDFs which is not under full theoretical control. Here the gluon saturation effects may be potentially important.

⁴ Here we use a glue constructed according to the prescription initiated in [39] and later updated in [40, 41], which we label as “KMR UGDF”. The KMR UGDF is available from the CASCADE Monte Carlo code [38].

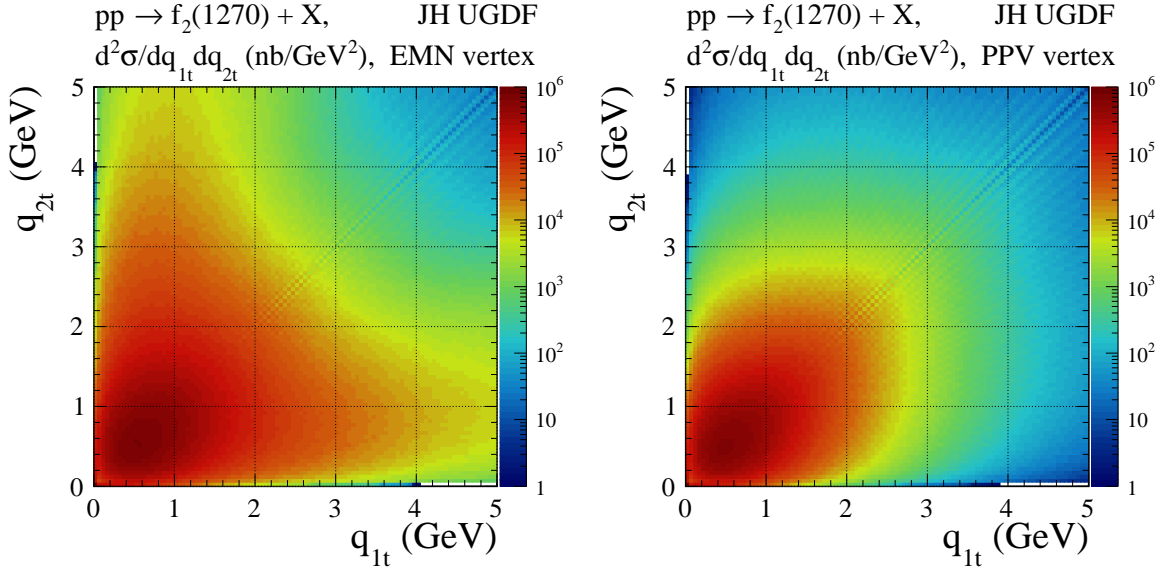


FIG. 6. Two-dimensional distributions in gluon transverse momenta for the JH UGDF and for two $g^*g^*f_2(1270)$ vertex prescription: EMN (left panel) and PPV (right panel). Here we used the dipole form factor (2.14) with $\Lambda_D = m_{f_2}$.

We have checked that

$$\frac{d^2\sigma_{\text{EMN}}}{dq_{1t}dq_{2t}} \left(\frac{d^2\sigma_{\text{PPV}}}{dq_{1t}dq_{2t}} \right)^{-1} \rightarrow 1, \quad \text{for } q_{1t} \rightarrow 0 \text{ and } q_{2t} \rightarrow 0, \quad (3.4)$$

i.e. the two vertices are equivalent for both on-shell gluons.

In Fig. 7 we show auxiliary distributions to discuss a possible role of the remaining terms in the $g^*g^*f_2$ PPV vertex (2.8) corresponding to helicities ($\Lambda = 0, L$) and ($\Lambda = 1$). Here we assumed the same Q^2 dependence of the form factor functions for all Λ terms; see Eqs. (2.10) and (2.14). The dominance of $\Lambda = 2$ term over $\Lambda = 0$ and $\Lambda = 1$ terms is certainly maintained at small values of Q_{ave}^2 and of p_t . However, the situation changes drastically at large gluon virtualities, i.e., the ($\Lambda = 1$) and ($\Lambda = 0, L$) structures of the $g^*g^*f_2$ vertex become equally important for $p_t > 2$ GeV.

Note that from the analysis of the $\gamma^*(Q_1^2)\gamma^*(Q_2^2) \rightarrow \pi\pi$ processes performed in [24, 25] it is clear that in the $f_2(1270)$ resonance region the helicity-(0, T) amplitude gives the dominant contribution and the other helicity projections become increasingly important for larger virtualities. From Fig. 5 of [24] and Fig. 3 of [25] we can see that for Q_1^2 fixed the helicity-1 contribution increases with increasing Q_2^2 while helicity-(0, L) contribution only slightly decreases. The situation changes when both photon virtualities are identical $Q_1^2 = Q_2^2$ and large, i.e. then the helicity-(0, L) component increases with increasing virtualities and becomes even larger than the helicity-1 component. This observation is consistent with our results presented in Fig. 7.

The theoretical results for the color-singlet gluon-gluon fusion underestimate the ALICE data especially for low- p_t region, $p_t < 2$ GeV. Does it mean that other mechanism(s) is (are) at the game?

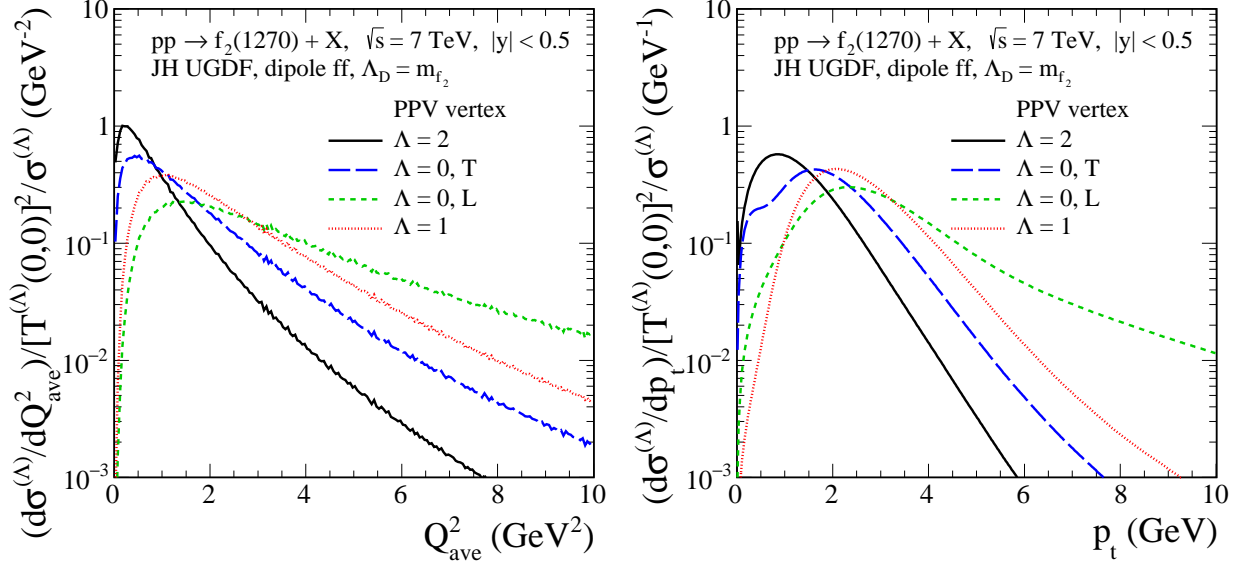


FIG. 7. Distributions normalized as explained in the y-axis in the averaged virtuality $Q_{\text{ave}}^2 = (Q_1^2 + Q_2^2)/2$ (left panel) and in the $f_2(1270)$ meson transverse momentum (right panel). Results for different $\Lambda = 0, 1, 2$ helicity terms in the $g^*g^*f_2$ vertex (2.8)–(2.10) using the same form of vertex form factors $F^{(\Lambda)}(Q_1^2, Q_2^2)$ (2.14) with $\Lambda_D = m_{f_2}$ are shown. In the calculation the JH UGDF was used.

In Fig. 8 we show the $\pi\pi$ rescattering contribution. Clearly the $\pi\pi \rightarrow f_2(1270)$ rescattering effect cannot describe the region of $p_t > 2$ GeV, where the gg -fusion mechanism is a possible explanation. In addition, we present the Born result (without absorptive corrections important only when restricting to purely exclusive processes) for the $pp \rightarrow pp f_2(1270)$ process proceeding via the pomeron-pomeron fusion mechanism calculated in the tensor-pomeron approach. For details regarding this approach we refer to [11, 43–45]. In the calculation we take the pomeron-pomeron- $f_2(1270)$ coupling parameters from [45].

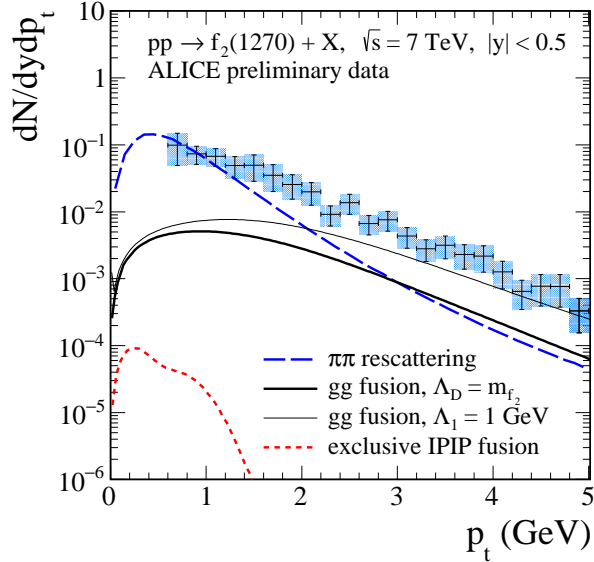


FIG. 8. Results for the $\pi\pi$ rescattering mechanism (long-dashed line), for the gg -fusion mechanism (solid lines), and for the pomeron-pomeron fusion mechanism (dotted line) together with the preliminary ALICE data from [2]. We show maximal contribution from the $\pi\pi$ rescattering as described in the main text. The results for the gg -fusion contributions were calculated for the JH UGDF and for the PPV vertex [helicity-2 plus helicity-(0, T) terms] and for two form factor functions (2.15) (top solid line) and (2.14) (bottom solid line). The dotted line corresponds to the Born-level result for the $pp \rightarrow pp f_2(1270)$ process via pomeron-pomeron fusion.

IV. CONCLUSIONS

In the present paper we have discussed production of $f_2(1270)$ tensor meson in proton-proton collisions. Two different approaches for the $\gamma^*\gamma^* \rightarrow f_2(1270)$ vertex, according to EMN (2.1) and PPV (2.8) parametrizations, have been considered. We have discussed their equivalence for both on-shell photons. We have checked that the energy-momentum tensor vertex, proposed in [3] [see Eq. (A1) of [3]], is equivalent to $\Gamma^{(2)}$ in the EMN vertex [see Eq. (2.3)] when ignoring the coupling constants. The coupling constants have been fixed by the Belle data for $\gamma\gamma \rightarrow f_2(1270) \rightarrow \pi\pi$. Then, the $g^*g^* \rightarrow f_2(1270)$ vertices have been obtained by replacing electromagnetic coupling constant by the strong coupling constant, modifying color factors and assuming a simple flavor structure of the $f_2(1270)$ isoscalar meson.

We have performed our calculation of the cross section for $pp \rightarrow f_2(1270) + X$ within the k_t -factorization approach. Two different unintegrated gluon distributions from the literature have been used. We have discussed corresponding uncertainties.

Our results have been compared to preliminary ALICE data presented in [2]. We have taken into account only the case when both gluons are transverse. At low $f_2(1270)$ transverse momenta the helicity-2 ($\Lambda = 2$) contribution dominates, while the helicity-0 ($\Lambda = 0, T$) is small, almost negligible, but competes with the $\Lambda = 2$ and even dominates at larger transverse momenta of $f_2(1270)$. In the PPV formalism there could be also $\Lambda = 0, L$ and $\Lambda = 1$ contributions which are difficult to fix by available data.

It has been shown that the results strongly depend on the form of the vertex form factor $F(Q_1^2, Q_2^2)$. With the GVDM form factor used previously in $\gamma^*\gamma \rightarrow f_2(1270)$ fusion [15, 16] one cannot describe the preliminary ALICE data. We have tried also other choices. With plausible form factor [e.g., dipole ansatz (2.14) with $\Lambda_D \simeq m_{f_2}$, factorized ansatz (2.15) with $\Lambda_1 \simeq 1$ GeV] one can describe the data for $p_t > 2$ GeV but it seems impossible to describe the low- p_t data. Clearly some mechanism at low- p_t must be in the game there.

We have shown that the final state $\pi\pi$ rescattering may be the missing candidate. A simple empirical model has been proposed. Adjusting corresponding probability for the $\pi\pi \rightarrow f_2(1270)$ rescattering and the Λ_D parameter in the dipole form factor for the $g^*g^* \rightarrow f_2$ vertex we have been able to describe the preliminary ALICE data.

The gluon saturation is expected at low x_1 and x_2 i.e. automatically rather low transverse momenta of $f_2(1270)$ where most probably the $\pi\pi$ rescattering dominates, which does not allow observation of saturation.

We have calculated also the exclusive production of $f_2(1270)$ meson via the pomeron-pomeron fusion mechanism with the parameters found in our previous analysis for the exclusive reaction $pp \rightarrow pp\pi^+\pi^-$. This contribution is concentrated at small $f_2(1270)$ transverse momenta but its role is rather marginal.

Our calculation suggest that the gluon-gluon fusion may be the dominant mechanism of the $f_2(1270)$ production at larger transverse momenta, $p_t > 3$ GeV. Other mechanisms are of course not excluded but it is clear that the gluon-gluon fusion is a very important mechanism which cannot be ignored in the analysis.

ACKNOWLEDGMENTS

We are indebted to Otto Nachtmann for a discussion of their approach. We are indebted to Graham Richard Lee for the discussion of the experimental data presented in his Ph.D. thesis [2]. A discussion with Philip Ilten on production of the $f_2(1270)$ meson in the current version of PYTHIA is acknowledged. We are also indebted to Marius Uthheim for explaining plans for including final state rescattering effects in the PYTHIA code for production of $\pi\pi$ resonances. This study was partially supported by the Polish National Science Centre under grant No. 2018/31/B/ST2/03537 and by the Center for Innovation and Transfer of Natural Sciences and Engineering Knowledge in Rzeszów (Poland).

-
- [1] J. Adams *et al.*, (STAR Collaboration), ρ^0 production and possible modification in Au+Au and p+p collisions at $\sqrt{s_{NN}} = 200$ GeV, Phys. Rev. Lett. **92** (2004) 092301, arXiv:nucl-ex/0307023 [nucl-ex].
 - [2] G. R. Lee, Ph.D. thesis: *Resonance production in the $\pi^+\pi^-$ decay channel in proton-proton collisions at 7 TeV*, University of Birmingham, 2016. http://www.hep.ph.bham.ac.uk/publications/thesis/grl_thesis.pdf.
 - [3] F. Fillion-Gourdeau and S. Jeon, *Tensor meson production in proton-proton collisions from the color glass condensate*, Phys. Rev. **C77** (2008) 055201, arXiv:0709.4196 [hep-ph].
 - [4] A. Cisek and A. Szczurek, *Prompt inclusive production of J/ψ , ψ' and χ_c mesons at the LHC in forward directions within the NRQCD k_t -factorization approach: Search for the onset of gluon saturation*, Phys. Rev. **D97** no. 3, (2018) 034035, arXiv:1712.07943 [hep-ph].

- [5] I. Babiarz, R. Pasechnik, W. Schäfer, and A. Szczurek, *Hadroproduction of scalar P-wave quarkonia in the light-front k_T -factorization approach*, JHEP **06** (2020) 101, arXiv:2002.09352 [hep-ph].
- [6] S. P. Baranov and A. V. Lipatov, *Prompt η_c meson production at the LHC in the NRQCD with k_T -factorization*, Eur. Phys. J. **C79** no. 7, (2019) 621, arXiv:1904.00400 [hep-ph].
- [7] I. Babiarz, R. Pasechnik, W. Schäfer, and A. Szczurek, *Prompt hadroproduction of $\eta_c(1S, 2S)$ in the k_T -factorization approach*, JHEP **02** (2020) 037, arXiv:1911.03403 [hep-ph].
- [8] P. Lebedowicz, R. Maciuła, and A. Szczurek, *Production of $f_0(980)$ meson at the LHC: Color evaporation versus color-singlet gluon-gluon fusion*, Phys. Lett. B **806** (2020) 135475, arXiv:2003.08200 [hep-ph].
- [9] V. Mathieu, A. Pilloni, M. Albaladejo, Ł. Bibrzycki, A. Celentano, C. Fernández-Ramírez, and A. Szczepaniak, (JPAC), *Exclusive tensor meson photoproduction*, Phys. Rev. D **102** no. 1, (2020) 014003, arXiv:2005.01617 [hep-ph].
- [10] M. Suzuki, *Tensor-meson dominance: Phenomenology of the f_2 meson*, Phys. Rev. **D47** (1993) 1043.
- [11] C. Ewerz, M. Maniatis, and O. Nachtmann, *A Model for Soft High-Energy Scattering: Tensor Pomeron and Vector Odderon*, Annals Phys. **342** (2014) 31, arXiv:1309.3478 [hep-ph].
- [12] S. Uehara *et al.*, (Belle Collaboration), *High-statistics measurement of neutral pion-pair production in two-photon collisions*, Phys. Rev. D **78** (2008) 052004, arXiv:0805.3387 [hep-ex].
- [13] M. R. Pennington, T. Mori, S. Uehara, and Y. Watanabe, *Amplitude analysis of high statistics results on $\gamma\gamma \rightarrow \pi^+\pi^-$ and the two photon width of isoscalar states*, Eur. Phys. J. C **56** (2008) 1, arXiv:0803.3389 [hep-ph].
- [14] L.-Y. Dai and M. R. Pennington, *Comprehensive amplitude analysis of $\gamma\gamma \rightarrow \pi^+\pi^-, \pi^0\pi^0$ and $\bar{K}K$ below 1.5 GeV*, Phys. Rev. D **90** no. 3, (2014) 036004, arXiv:1404.7524 [hep-ph].
- [15] N. N. Achasov and V. A. Karnakov, *Vector Meson Dominance Model in $\gamma + \gamma^*(Q^2) \rightarrow f(1270, 2^+) \rightarrow \pi\pi$* , Z. Phys. C **30** (1986) 141.
- [16] N. N. Achasov, A. V. Kiselev, and G. N. Shestakov, *Study of the $f_2(1270)$ and $a_2(1320)$ resonances in $\gamma^*(Q^2)\gamma$ collisions*, JETP Lett. **102** no. 9, (2015) 571, arXiv:1509.09150 [hep-ph]. [Pisma Zh. Eksp. Teor. Fiz.102,no.9,655(2015)].
- [17] V. M. Braun and N. Kivel, *Hard exclusive production of tensor mesons*, Phys. Lett. B **501** (2001) 48, arXiv:hep-ph/0012220.
- [18] V. M. Braun, N. Kivel, M. Strohmaier, and A. A. Vladimirov, *Electroproduction of tensor mesons in QCD*, JHEP **06** (2016) 039, arXiv:1603.09154 [hep-ph].
- [19] G. A. Schuler, F. A. Berends, and R. van Gulik, *Meson-photon transition form factors and resonance cross-sections in e^+e^- collisions*, Nucl. Phys. B **523** (1998) 423, arXiv:hep-ph/9710462.
- [20] M. Hoferichter and P. Stoffer, *Asymptotic behavior of meson transition form factors*, JHEP **05** (2020) 159, arXiv:2004.06127 [hep-ph].
- [21] M. Masuda *et al.*, (Belle Collaboration), *Study of π^0 pair production in single-tag two-photon collisions*, Phys. Rev. **D93** no. 3, (2016) 032003, arXiv:1508.06757 [hep-ex].
- [22] V. Pascalutsa, V. Pauk, and M. Vanderhaeghen, *Light-by-light scattering sum rules constraining meson transition form factors*, Phys. Rev. **D85** (2012) 116001, arXiv:1204.0740 [hep-ph].
- [23] M. Poppe, *Exclusive Hadron Production in Two Photon Reactions*, Int. J. Mod. Phys. **A1** (1986) 545.
- [24] M. Hoferichter and P. Stoffer, *Dispersion relations for $\gamma^*\gamma^* \rightarrow \pi\pi$: helicity amplitudes, subtractions, and anomalous thresholds*, JHEP **07** (2019) 073, arXiv:1905.13198 [hep-ph].
- [25] I. Danilkin, O. Deineka, and M. Vanderhaeghen, *Dispersive analysis of the $\gamma^*\gamma^* \rightarrow \pi\pi$ process*, Phys. Rev. D **101** no. 5, (2020) 054008, arXiv:1909.04158 [hep-ph].

- [26] D. V. Shirkov and I. L. Solovtsov, *Analytic Model for the QCD Running Coupling with Universal $\bar{\alpha}_s(0)$ Value*, Phys. Rev. Lett. **79** (1997) 1209, arXiv:hep-ph/9704333 [hep-ph].
- [27] B. Abelev *et al.*, (ALICE Collaboration), *Neutral pion and η meson production in proton-proton collisions at $\sqrt{s} = 0.9$ TeV and $\sqrt{s} = 7$ TeV*, Phys.Lett. **B717** (2012) 162, arXiv:1205.5724 [hep-ex].
- [28] R. Maciuła, A. Szczurek, and A. Cisek, *J/ψ -meson production within improved color evaporation model with the k_T -factorization approach for $c\bar{c}$ production*, Phys. Rev. D **99** no. 5, (2019) 054014, arXiv:1810.08063 [hep-ph].
- [29] S. Pratt and S. Petriconi, *Alternative size and lifetime measurements for high-energy heavy ion collisions*, Phys. Rev. **C68** (2003) 054901, arXiv:nucl-th/0305018 [nucl-th].
- [30] S. Pratt, *Shapes and Sizes from Non-Identical-Particle Correlations*, Braz. J. Phys. **37** (2007) 871–876, arXiv:nucl-th/0612006 [nucl-th].
- [31] T. Sjöstrand and M. Uthm, *A Framework for Hadronic Rescattering in pp Collisions*, arXiv:2005.05658 [hep-ph].
- [32] G. Antchev *et al.*, (TOTEM Collaboration), *Measurement of proton-proton elastic scattering and total cross-section at $\sqrt{s} = 7$ TeV*, EPL **101** no. 2, (2013) 21002.
- [33] G. Aad *et al.*, (ATLAS Collaboration), *Measurement of the total cross section from elastic scattering in pp collisions at $\sqrt{s} = 7$ TeV with the ATLAS detector*, Nucl. Phys. **B889** (2014) 486, arXiv:1408.5778 [hep-ex].
- [34] F. Hautmann and H. Jung, *Transverse momentum dependent gluon density from DIS precision data*, Nucl. Phys. **B883** (2014) 1, arXiv:1312.7875 [hep-ph].
- [35] M. Ciafaloni, *Coherence effects in initial jets at small Q^2/s* , Nucl. Phys. **B296** (1988) 49.
- [36] S. Catani, F. Fiorani, and G. Marchesini, *QCD coherence in initial state radiation*, Phys. Lett. **B234** (1990) 339.
- [37] S. Catani, F. Fiorani, and G. Marchesini, *Small- x behavior of initial state radiation in perturbative QCD*, Nucl. Phys. **B336** (1990) 18.
- [38] H. Jung *et al.*, *The CCFM Monte Carlo generator CASCADE version 2.2.03*, Eur. Phys. J. **C70** (2010) 1237, arXiv:1008.0152 [hep-ph].
- [39] M. A. Kimber, A. D. Martin, and M. G. Ryskin, *Unintegrated parton distributions*, Phys. Rev. **D63** (2001) 114027, arXiv:hep-ph/0101348 [hep-ph].
- [40] G. Watt, A. D. Martin, and M. G. Ryskin, *Unintegrated parton distributions and electroweak boson production at hadron colliders*, Phys. Rev. **D70** (2004) 014012, arXiv:hep-ph/0309096 [hep-ph]. [Erratum: Phys. Rev.D70,079902(2004)].
- [41] A. D. Martin, M. G. Ryskin, and G. Watt, *NLO prescription for unintegrated parton distributions*, Eur. Phys. J. **C66** (2010) 163, arXiv:0909.5529 [hep-ph].
- [42] M. Glück, P. Jimenez-Delgado, E. Reya, and C. Schuck, *On the role of heavy flavor parton distributions at high energy colliders*, Phys.Lett. **B664** (2008) 133, arXiv:0801.3618 [hep-ph].
- [43] P. Lebiedowicz, O. Nachtmann, and A. Szczurek, *Exclusive central diffractive production of scalar and pseudoscalar mesons; tensorial vs. vectorial pomeron*, Annals Phys. **344** (2014) 301, arXiv:1309.3913 [hep-ph].
- [44] P. Lebiedowicz, O. Nachtmann, and A. Szczurek, *Central exclusive diffractive production of the $\pi^+\pi^-$ continuum, scalar, and tensor resonances in pp and $p\bar{p}$ scattering within the tensor Pomeron approach*, Phys. Rev. **D93** (2016) 054015, arXiv:1601.04537 [hep-ph].
- [45] P. Lebiedowicz, O. Nachtmann, and A. Szczurek, *Extracting the Pomeron-Pomeron- $f_2(1270)$ coupling in the $pp \rightarrow pp\pi^+\pi^-$ reaction through the angular distribution of the pions*, Phys. Rev. D **101** no. 3, (2020) 034008, arXiv:1901.07788 [hep-ph].